Thermal Mode Spectroscopy for Thermal Diffusivity of Millimeter-Size Solids

Hirotsugu Ogi,* Tatsuya Ishihara, Hideshi Ishida, Akira Nagakubo, Nobutomo Nakamura, and Masahiko Hirao
Graduate School of Engineering Science, Osaka University, Toyonaka, Osaka 560-8531, Japan
(Received 6 April 2016; published 4 November 2016)

Heat conduction possesses (thermal) modes in analogy with acoustics even without oscillation. Here, we establish thermal mode spectroscopy to measure the thermal diffusivity of small specimens. Local heating with a light pulse excites such modes that show antinodes at the heating point, and photothermal detection at another antinode spot allows measuring relaxation behavior of the desired mode selectively: The relaxation time yields thermal diffusivity. The Ritz method is proposed for arbitrary geometry specimens. This method is applicable even to a diamond crystal with ~1 mm dimensions.

DOI: 10.1103/PhysRevLett.117.195901

Thermal conductivity κ, the proportionality factor between the heat flux density and temperature gradient in Fourier's law, is an important parameter in condensed matter physics. Dynamically, it governs heat diffusion behavior based on the heat equation:

$$\frac{\partial T}{\partial t} - \frac{\kappa}{C\rho}\nabla^2 T = 0. \quad (1)$$

Here, T, t, C, and ρ denote the temperature, time, specific heat, and mass density, respectively. Many methods were proposed for measuring thermal conductivity. Statically, it was determined by measuring the temperature gradient in a specimen with a known power input [1–3]. However, such a steady-state approach needs sufficiently large specimens. For smaller specimens, it has been dynamically evaluated using the heat-transport phenomenon with Eq. (1); heating a specimen periodically [4–9] or transiently [10–13] and detecting the temperature change at a specific point, the thermal diffusivity $\alpha = \kappa/C\rho$ was extracted by comparing the measured temperature response with the corresponding theoretical model, and then κ was obtained from a known specific heat and mass density.

All the existing dynamic methods use the *propagation* of heat and require the condition that the heat diffusive wavelength must be adequately smaller than the specimen dimension. This requirement prevents us from determining thermal conductivity with high accuracy for very small specimens. The ultrafast pump-probe laser method was proposed for local thermal diffusivity, but coatings needed for the heat source and heat detection for transparent materials highly affected the thermal diffusivity measurement because of a large contribution of the interface conductance to heat resistance in such a localized region [14].

In this Letter, we propose a very simple but accurate method for measuring the thermal diffusivity of small solids based on a new concept, *thermal mode in heat conduction*. To understand its essence, it is helpful to compare this method with acoustic resonance. For measuring the elastic constants of a solid, one uses the pitch-catch method, for example, where the traveling time and distance of an elastic wave are measured to determine the sound velocity and the corresponding elastic constant with a known mass density. This method thus uses the propagation of sound and is therefore inapplicable to small specimens because of the overlapping of pulse echoes; the specimen must be larger than the wavelength of the sound. (This limitation is equivalent to that in the existing dynamic methods for thermal diffusivity as mentioned above.) An acoustic resonance method has been alternatively used for such a tiny specimen: A natural resonance frequency of a solid provides us with the effective elastic constant with known dimensions and mass density. Thus, the acoustic resonance method uses *vibrational modes* and becomes more effective for smaller specimens, where acoustic energy is well confined to excite the modes strongly. Measuring many resonance frequencies allows us to determine all the independent elastic constants of small solids, known as resonant ultrasound spectroscopy [15,16]. Note that the mode identification becomes the key for the successful determination of the elastic constants in the resonance method [17,18]. The proposed method in this Letter corresponds to the resonance method in acoustics; it is effective even for smaller specimens, but correct mode identification is required.

Compared with the damped wave equation, the heat equation [Eq. (1)] can be regarded as the wave equation with a quite large damping system, where the inertia term becomes negligible. (Heat conduction actually behaves like sound under special conditions, known as the second sound [19,20], but this is not the present case.) This means the overdamping of heat vibration, and there are modes for heat conduction, analogous with acoustic vibrational modes, even without vibration in the heat flow. Supplemental Movies 1 and 2 explicitly demonstrate this phenomenon. [They are calculated with a finite volume method (FVM) as shown in Supplemental Material [21].] When the heat pulse is applied at the center point on the shorter edge side of a rectangular parallelepiped, the temperature increase dominantly occurs along the shorter edge (Movie 1) as if there were a boundary inside the specimen along the shorter side, whereas when it is applied on the center, the temperature preferentially increases in the median zone along the

shorter edge direction (Movie 2). More importantly, the relaxation time τ for equilibrium after the excitation is different from each other; it is longer for the edge-heating case. Thus, the relaxation time and the temperature distribution are dependent on the location of the impulsive heating source, and they correspond to the eigenvalue and eigenfunction of the thermal mode, respectively, being analogous to the resonant frequency (eigenvalue) and vibration pattern (eigenfunction) in acoustics. Because τ is directly related to α through unambiguous parameters, we can determine α and then κ by selectively exciting a single thermal mode and measuring its relaxation time.

Here, we develop a pump-probe laser technique for achieving the mode-selective excitation and detection of thermal modes. An impulsive and localized heating on a specimen could excite various thermal modes. Each mode relaxes with its specific relaxation time (eigenvalue) and temperature-change pattern (eigenfunction). Mode identification is therefore important in this process, and we attained this by excitation and detection at antinodal points of the desired mode. We confirm this principle with both a numerical simulation and experiment and demonstrate the high applicability of the thermal mode spectroscopy to small specimens with high thermal conductivities, including monocrystal diamond. Furthermore, the Ritz method analysis has been established for arbitrary geometry specimens.

The thermal modes are analytically calculated for a rectangular parallelepiped. Because the relaxation time is much shorter than the time needed for the heat transfer toward outside through the boundary for small and high thermal-conductivity materials, the adiabatic boundary condition is well applicable as will be discussed later. The general solution of Eq. (1) in this case takes the form

$$T(\mathbf{r},t)=\sum_{l,m,n\geq 0} A^{\pm}_{lmn}\exp(\pm i\mathbf{k}\cdot\mathbf{r})\exp\left(-\frac{t}{\tau_{lmn}}\right). \quad (2)$$

Here, l, m, and n are integers showing the mode order. $\mathbf{k}=(k_l,k_m,k_n)=(l\pi/L_1,m\pi/L_2,n\pi/L_3)$ denotes the spatial wave number vector, and L_i is the side length along the x_i axis. $A^{\pm}_{lmn}$ are amplitudes for individual modes. τ_{lmn} represents the relaxation time of mode (lmn), and it is given by

$$\tau^{-1}_{lmn}=\alpha(k_l^2+k_m^2+k_n^2). \quad (3)$$

Supplemental Fig. S1 shows the relaxation time for each mode and corresponding temperature distributions (mode figures) for the first 12 thermal modes of an aluminum rectangular parallelepiped. (In this study, we assign the mode number from the longest-relaxation-time mode in order, except for the zeroth mode of the steady state.) The red region indicates the antinode of the thermal mode, where a large temperature change occurs. The blue region indicates the node of the thermal mode, where the minimum temperature change occurs. Therefore, if we can measure the relaxation time of one of them, the thermal diffusivity is simply obtained from Eq. (3) with measurable dimensions.

Materials with high thermal conductivities often exhibit ultrahigh hardness, and it is difficult to machine them into rectangular parallelepipeds. We, therefore, propose the Ritz method for analyzing the thermal mode in order to apply thermal mode spectroscopy to solids with arbitrary shapes. The temperature in Eq. (1) is expressed by $T(\mathbf{r},t)=f(\mathbf{r})e^{-t/\tau}$, yielding $[\nabla^2+(\tau\alpha)^{-1}]f=0$. Using the functional differential method, we have

$$\begin{aligned}\delta\Pi &\equiv \int_V\left(\frac{1}{\tau\alpha}f+\nabla^2 f\right)\delta f dV \\ &= \frac{1}{\tau\alpha}\int_V f\cdot\delta f dV-\int_V(\nabla f)\cdot(\nabla\delta f)dV, \end{aligned} \quad (4)$$

where the adiabatic boundary condition (grad $f=0$) was used at the boundary in performing the partial integral for the second term. We expand f with many basis functions ϕ_i as $f(\mathbf{r})=\sum a_i\phi_i(\mathbf{r})$ with the weighting constants a_i, and, using the variational principle $\partial\Pi/\partial a_i=0$, an eigenvalue equation is obtained:

$$\left(\frac{1}{\tau\alpha}\mathbf{M}-\mathbf{\Gamma}\right)\mathbf{a}=0, \quad (5)$$

where components of the matrices $\mathbf{M}$ and $\mathbf{\Gamma}$ are calculated by the basis functions as

$$M_{ij}=\int_V\phi_i\phi_j dV, \qquad \Gamma_{ij}=\int_V\frac{\partial\phi_i}{\partial x_k}\frac{\partial\phi_j}{\partial x_k}dV. \quad (6)$$

Therefore, from the eigenvalue in Eq. (5), $1/\tau\alpha$, we obtain the thermal diffusivity through the measured relaxation time, and from the eigenvector $\mathbf{a}$ we obtain the temperature distribution of each mode. We used a power series for the basis functions as $\phi_i=x_1^p x_2^q x_3^r$, which have been adopted in calculating resonance frequencies in resonance ultrasound spectroscopy [15,24].

For checking the accuracy of this algorithm, we calculated the relaxation time with the Ritz method from Eq. (5) and compared it with the exact solution from Eq. (3) for a rectangular parallelepiped (see Supplemental Material for the volume integration [21]). By using a sufficiently larger number of basis functions of $p+q+r\leq 10$, they showed excellent agreements within 0.001% differences for the first ten modes. Figure 1 shows the relaxation time and corresponding figures on the inclined plane for the aluminum triangular pyramid in Table I calculated from Eq. (5). (Note that an analytical solution is unavailable for this shape.) Modes 3 and 6 show discriminative temperature patterns [Figs. 1(d) and 1(g)], and we use them for the experiment below.

Specimens used in this study are rectangular parallelepipeds of aluminum, copper, nickel, and monocrystal diamond (type IIa), and the triangular pyramid of aluminum with the orthogonal apex as illustrated in Fig. 1(a). Their dimensions are comparable with each other. Concerning the diamond specimen, we made a black-body thin film around the heating points and a 300-nm Pt thin film around the detection points because of its high transparency. They are so small that conventional methods will fail to measure their thermal conductivities with high accuracy.

For confirming the mode-selective principle, three-dimensional numerical simulations based on the FVM (see Supplemental Material [21]) were performed for the

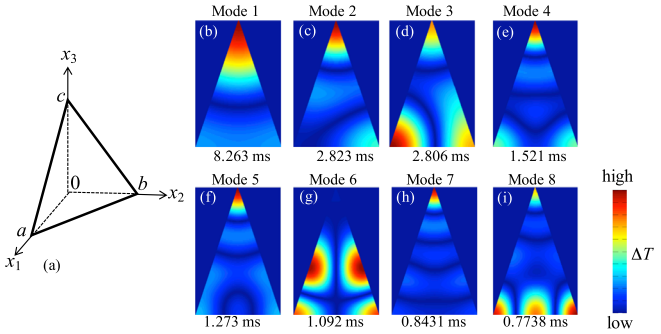

FIG. 1. Thermal modes of the aluminum triangular pyramid. The Ritz method was used to calculate the relaxation time and corresponding temperature distribution of the tetrahedron with the dimensions in Table I. (a) Schematic of the specimen shape. Dimensions a, b, and c are shown in Table I. (b)–(i) Distributions of the absolute value of the temperature change on the inclined plane from modes 1 to 8.

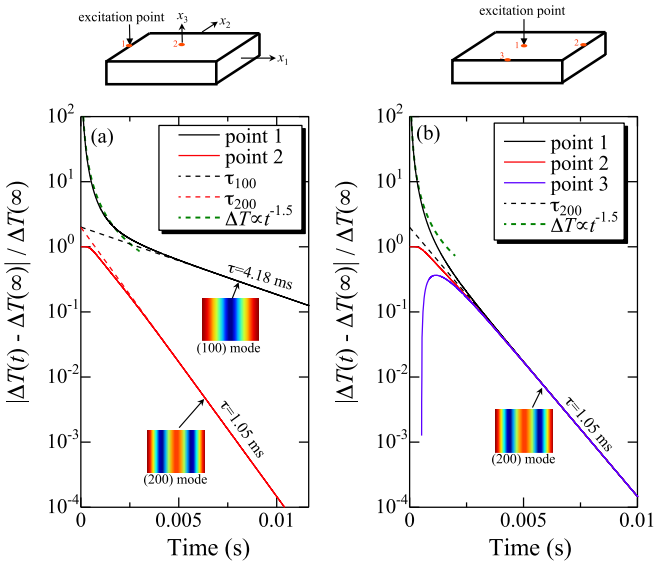

FIG. 2. Numerical simulation of a surface-temperature change caused by a heat pulse. The heat pulse is applied (a) on the center of the edge side along the x_2 axis and (b) on the surface center, and temperature evolutions at characteristic points (shown in the upper illustrations with red circles) are shown. The green broken lines indicate the solution of the bulk diffusion. The relaxation-time values determined by fitting the exponential function to the simulated data are shown. The mode figures are also shown. $\Delta T(t) = T(t) - T(0)$ denotes the temperature change.

aluminum rectangular parallelepiped shown in Fig. S1(a) under the adiabatic boundary condition. A heat pulse was locally injected on the top surface, and the temperature changes on other points were calculated. The results are shown in Fig. 2. When the heat pulse is applied on the center edge along the x_2 direction [Fig. 2(a)], the temperature at the same point (point 1) steeply drops and then follows an exponential function with the relaxation time of 4.18 ms. We find that the initial steep drop follows the relation $\Delta T \propto t^{-1.5}$, which agrees with the solution of the bulk diffusion into infinite space. The exponential decay well agrees with the relaxation time of the (100) mode ($\tau_{100} = 4.20$ ms), whose antinode exists at the excitation and detection point as shown in Fig. S1(b). The temperature change at point 2, however, follows the exponential decay with the relaxation time of mode (200), where the antinodes appear at both the excitation and detection points [Fig. S1(e)]. (Higher modes, exhibiting antinodes at excitation points, are excited as well, but they disappear quickly because of their much shorter relaxation time and less affect the relaxation behavior of lower modes.) When the heat pulse is applied on the center [Fig. 2(b)], the temperature at the same point again initially obeys the $t^{-1.5}$ law and then follows the exponential decay with the relaxation time of 1.05 ms, which is identical to τ_{200}, whose antinode exists at the excitation and detection points [Fig. S1(e)]. The temperature changes at points 2 and 3 also show a relaxation time very close to τ_{200}, because their excitation and detection points are involved in the antinodes of the (200) mode. Thus, a specific mode will be selectively measured by applying the heat pulse and detecting the temperature at antinodes in its mode figure.

Supplemental Fig. S2 shows the optics developed for the mode-selective thermal mode spectroscopy. We used the pump light pulse with a 1064 nm wavelength. Its duration is about 100 μs. The power of the single pulse was ~3 mJ, and the repetition rate was 1 Hz. For the detection of the local temperature change, we used a titanium-sapphire pulse laser with an 800 nm wavelength and 150 fs duration. The repetition rate was 80 MHz, which is high enough compared with the relaxation rate of thermal mode (< ~8 kHz), making it possible to monitor the temperature change nearly continuously through the thermo-optical interaction. Note that we do not need to measure the absolute temperature value but the relative temperature change, that is proportional to the reflectivity change ΔR of the probe light, to obtain the relaxation time. Details appear in Supplemental Material [21].

Supplemental Fig. S3 shows relaxation curves of the fundamental mode measured for the rectangular parallelepipeds in Table I. The broken lines in Fig. S3(b) show the relaxation curves calculated with the reported thermal properties in Table I; they show good agreements with the experiments. We measured the relaxation curves with various positions for the excitation and detection for the aluminum specimen for selectively measuring (100), (010), and (200) modes as shown in Supplemental Fig. S4, showing good agreements with the theory. Figures 3(a) and 3(b) also compare the relaxation curves for two different modes for the aluminum tetrahedron specimen and the monocrystal diamond specimen. The measurements are again consistently explained with the Ritz method calculation and theory, respectively. Thus, these results robustly confirm the mode-selective excitation and detection in thermal mode spectroscopy. The error for the relaxation-time measurement depended on the specimen; it was about 5% for the aluminum specimen and 14% for the diamond specimen, for example. Table I shows thermal conductivities determined from the measured relaxation curves (κ_{exp}), which are reasonably coincident with the reported values (κ_{rep}).

TABLE I. Dimensions L_i along the x_i axis (mm), mass density ρ (g/cm^3), specific heat capacity C (J/kg K), the relaxation-time ratio τ_{100}/τ_h, minimum modulation frequency $f_{\min}$ (Hz), inverse relaxation time for the (200) mode f_{200} (Hz), thermal conductivity determined here $\kappa_{\exp}$ (W/m K), and that reported previously κ_{rep} (W/m K). (a) From Ref. [25].(b) From Ref. [10]. (c) Taken from Ref. [26] at 273 K. (d) From Ref. [27]. (e) From Ref. [28]. (f) From Ref. [29]. (g) Calculated from thermal diffusivity data in Ref. [30] with the mass density and specific heat capacity in Table I. (h) From Ref. [31]. (i) From Ref. [32]. (j) Side dimensions a, b, and c of the tetrahedron in Fig. 1(a), respectively.

Materials	L_1	L_2	L_3	ρ	C	$\tau_{100}/\tau_h(10^{-5})$	$f_{\min}$	f_{200}	$\kappa_{\exp}$	κ_{rep}
Al	1.985	1.491	1.236	2.70	902[a]	1.4	10	982	240 ± 12	222[b], 235[c]
Al(tetra.)	1.898[j]	1.918[j]	3.858[j]			1.8	4	350	247 ± 13	
Cu	1.504	0.981	0.626	8.94	385[d]	0.9	47	2020	386 ± 18	398[e], 410[b]
Ni	1.551	0.953	0.629	8.91	451[f]	5.8	8	368	75.0 ± 5.4	67[b], 84[g]
Diamond	2.464	2.444	0.549	3.51	510[h]	0.5	370	7940	1905 ± 266	2180[i]

A successful observation of the thermal mode requires a high adiabatic degree at the boundary; the heat conduction within the specimen should dominate the relaxation phenomenon compared with the heat leakage outside. This can be evaluated by comparing the relaxation time for heat conduction inside the specimen and that for the heat transfer to outside. The heat flow across the boundary with area A is expressed by $hA(T_s - T_o)$ with the heat transfer coefficient h, where T_s and T_o denote the surface temperature and the constant outside temperature, respectively. The relative surface temperature $\tilde{T}_s \equiv T_s - T_o$ changes with time, following the heat balance equation: $\rho CV(d\tilde{T}_s/dt) = -hA\tilde{T}_s$ with volume V. Thus, the relaxation time τ_h, due to the heat transfer to outside, is estimated by $\tau_h = \rho CL/h$, where L denotes the representative specimen length ($= L_3$). Assuming a typical value of $h = 10$ W/m^2 K for the natural convection of air, the ratio τ_{100}/τ_h is calculated in Table I, which is of the order of 10^{-5} or less. [This ratio is proportional to the so-called Biot number ($= hL/\kappa$).] Therefore, the heat transfer to outside can be negligible during the relaxation of thermal modes.

The specimens used here are fairly small, and a very high modulation frequency ω would be needed to evaluate their thermal conductivities with the existing methods. The validity of the modulation frequency has been evaluated by the thermal-diffusivity wavelength $\lambda(= \sqrt{\alpha/\omega})$; the minimum modulation frequency $f_{\min}$ was estimated by substituting the minimum dimension for λ. However, we insist that this evaluation is inappropriate for a specimen with smaller in-plane dimensions: Most previous experiments had been performed on the center surface region by applying heat sources. In this situation, the higher thermal modes would be excited. [For example, the (200) mode shows the antinode on the center region as seen in Fig. S1(e).] Therefore, the modulation frequency must be significantly higher than the relaxation rate of the (200) mode, $f_{200} = 1/\tau_{200}$; otherwise, the measurements will feel the boundary, and the one- or two-dimensional models for the infinity half space would fail. As shown in Table I, f_{200} is much higher than $f_{\min}$, and measurements based on $f_{\min}$ could be unreliable. For example, the thermal conductivity of diamond was evaluated by the 3ω method with a modulation frequency higher than ~50 Hz [7]. The τ_{200} value for their specimen is, however, estimated to be ~0.3 ms, resulting in $f_{200} \sim 3000$ Hz. Thus, the modulation frequency could be significantly lower than or comparable to the relaxation rate, and the measurement might have been affected by the thermal mode.

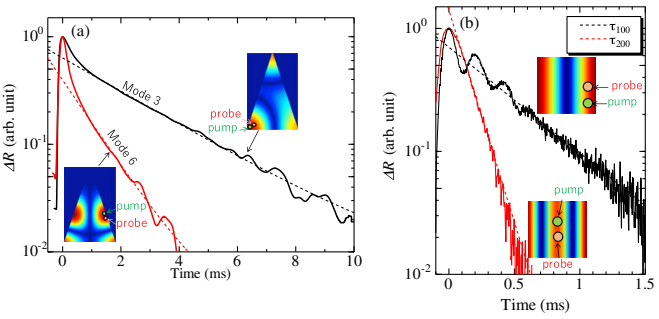

FIG. 3. Mode-selective measurements. (a) Relaxation curves for mode 3 and mode 6 of the aluminum tetrahedron in Table I. Broken lines are relaxation curves calculated by the Ritz method. (b) Comparison between measured (solid lines) and theoretical (broken lines) relaxation curves of the τ_{100} and τ_{200} modes for the monocrystal diamond in Table I. The mode figures for the temperature change and excitation and detection points are illustrated. The oscillations in the relaxation curves are background signals caused by the laser-power fluctuation in the probe light, which appeared irregularly.

We investigated the effects of the added thin film and the interface conductance at the film-specimen interface on the relaxation time. Our numerical calculation reveals that they hardly affect the relaxation time when the thickness ratio between the film and specimen is smaller than ~1% as shown in Supplemental Fig. S5, which is well satisfied in the experiments (the thickness ratio between the Pt thin film and diamond is about 0.06%).

It is important to note that the thermal mode spectroscopy is little affected by the temperature variation inside the specimen. For example, in the rectangular parallelepiped aluminum specimen in Table I, the final temperature increase $[\Delta T(\infty)]$ of the specimen is estimated to be only 0.017 K with a 3 mJ excitation pulse and a reflectance of 0.95 at 1064 nm wavelength. As shown in Fig. 2, the temperature increase inside the specimen $\Delta T(t)$ remains smaller than $2\Delta T(\infty)$ during relaxation procedures. The local and

transient temperature increase at the excitation point fails to affect the relaxation constant, because we do not use the data just after the excitation. Therefore, the measurable thermal diffusivity is almost equivalent to that at the base temperature before the heat-pulse excitation, $T(0)$, because of the low excitation energy. On the other hand, the base temperature $T(0)$ can be controlled through heat transfer or heat radiation, which, however, do not affect the relaxation time of thermal modes as discussed above.

We finally discuss the applicability of our analysis for ultrasmall specimens. When the specimen dimension is comparable to or smaller than the phonon mean free path, Fourier's law fails to explain the relaxation phenomenon and the ballistic conduction becomes dominant [33], where alternative (or extended) basic equations should be considered [34,35]. The incorporation of the ballistic conduction will apparently decrease the thermal diffusivity, leading to a longer relaxation time. Our analysis becomes inapplicable for such an ultrasmall specimen, and we need to perform the mode analysis in the extended equations, which will be our future work.

In summary, we established a very simple but accurate method for evaluating the thermal conductivity of small solids using the thermal mode, whose importance has been unnoticed. The mode-control measurement is the key, and this was achieved by applying a heat pulse and detecting the temperature change at the antinodal points. Even a higher mode with a shorter relaxation time ($\sim$100 μs) of the diamond specimen was clearly observed [Fig. 3(b)], indicating the applicability of this method to small and high thermal conductivity solids like diamonds. It is also applicable to thermally anisotropic materials by measuring multiple relaxation curves, so that anisotropic thermal conductivities will be determined from a single small specimen (Supplemental Material [21]). Furthermore, the thermal mode will give an unambiguous definition for the thermal diffusivity of composite materials. Whereas thermal diffusivity evaluated by a propagation-based method will correspond to the group velocity in acoustics, that evaluated by the thermal mode will yield an intrinsic thermal diffusivity like the phase velocity in acoustics.

The authors are grateful to Professor H. J. Maris (Brown University) for valuable comments on this study. The diamond specimen was supplied by Dr. H. Sumiya (Sumitomo Electric Industries, Ltd.). H. O. established the thermal mode spectroscopy, developed the optics, and wrote the Letter. T. I. measured the relaxation curves. H. I. performed the finite-volume-method simulations. A. N., N. N., and M. H. contributed to the development of optics.

*ogi@me.es.osaka-u.ac.jp

[1] M. J. Laubitz, *Thermal Conductivity* (Academic, London, 1969), Vol. I, pp. 111–185.
[2] N. S. Rasor and J. D. McClelland, Rev. Sci. Instrum. **31**, 595 (1960).
[3] D. Kraemer and G. A. Chen, Rev. Sci. Instrum. **85**, 025108 (2014).
[4] R. W. King, Phys. Rev. **6**, 437 (1915).
[5] C. Starr, Rev. Sci. Instrum. **8**, 61 (1937).
[6] D. G. Cahill, Rev. Sci. Instrum. **61**, 802 (1990).
[7] J. R. Olson, R. O. Pohl, J. W. Vandersande, A. Zoltan, T. R. Anthony, and W. F. Banholzer, Phys. Rev. B **47**, 14850 (1993).
[8] C. C. Ghizoni and L. C. M. Miranda, Phys. Rev. B **32**, 8392 (1985).
[9] M. Chirtoc and G. Mihăilescu, Phys. Rev. B **40**, 9606 (1989).
[10] W. J. Parker, R. J. Jenkins, C. P. Butler, and G. L. Abbott, J. Appl. Phys. **32**, 1679 (1961).
[11] M. Golombok and L. C. Shirvill, J. Appl. Phys. **63**, 1971 (1988).
[12] W. S. Capinski, H. J. Maris, T. Ruf, M. Cardona, K Ploog, and D. S. Katzer, Phys. Rev. B **59**, 8105 (1999).
[13] A. J. Schmidt, X. Chen, and G. Chen, Rev. Sci. Instrum. **79**, 114902 (2008).
[14] R. J. Stoner and H. J. Maris, Phys. Rev. B **48**, 16373 (1993).
[15] A. Migliori, J. L. Sarrao, W. M. Visscher, T. M. Bell, M. Lei, Z. Fisk, and R. G. Leisure, Physica (Amsterdam) **183B**, 1 (1993).
[16] J. Maynard, Phys. Today **49**, No. 1, 26 (1996).
[17] H. Ogi, H. Ledbetter, S. Kim, and M. Hirao, J. Acoust. Soc. Am. **106**, 660 (1999).
[18] H. Ogi, K. Sato, T. Asada, and M. Hirao, J. Acoust. Soc. Am. **112**, 2553 (2002).
[19] H. E. Jackson, C. T. Walker, and T. F. McNelly, Phys. Rev. Lett. **25**, 26 (1970).
[20] C. I. Christov and P. M. Jordan, Phys. Rev. Lett. **94**, 154301 (2005).
[21] See Supplemental Material at http://link.aps.org/supplemental/10.1103/PhysRevLett.117.195901 for measurement details, volume integration, and finite volume method simulation, which includes Refs. [22, 23].
[22] G. D. Smith, *Numerical Solution of Partial Differential Equations* (Oxford University Press, New York, 1965).
[23] S. V. Patankar, *Numerical Heat Transfer and Fluid Flow* (Taylor & Francis, London, 1980).
[24] W. M. Visscher, A. Migliori, T. M. Bell, and R. A. Reinert, J. Acoust. Soc. Am. **90**, 2154 (1991).
[25] E. H. Buyco and F. E. Davis, J. Chem. Eng. Data **15**, 518 (1970).
[26] *American Institute of Physics Handbook*, 3rd ed., edited by D. E. Gray (McGraw-Hill, New York, 1972).
[27] G. K. White and S. J. Collocott, J. Phys. Chem. Ref. Data **13**, 1251 (1984).
[28] A. J. Walter and A. R. Trowell, J. Mater. Sci. **6**, 1044 (1971).
[29] K. E. Grew, Proc. R. Soc. A **145**, 509 (1934).
[30] C. A. Paddock and G. L. Eesley, J. Appl. Phys. **60**, 285 (1986).
[31] A. C. Victor, J. Chem. Phys. **36**, 1903 (1962).
[32] D. G. Onn, A. Witek, Y. Z. Qiu, T. R. Anthony, and W. F. Banholzer, Phys. Rev. Lett. **68**, 2806 (1992).
[33] H. B. G. Casimir, Physica (Utrecht) **5**, 495 (1938).
[34] A. Majumdar, J. Heat Transfer **115**, 7 (1993).
[35] G. Chen, Phys. Rev. B **57**, 14958 (1998).